Academic Journal of Sukuna – AJoS, A Peer-reviewed Interdisciplinary Journal
Volume 5 (Issue 1) 2025 July (2082 Ashad), Pp. 100– 118, ISSN 2594-3138 (Print)
Research Management Cell (RMC – Sukuna), Sundarharaincha, Morang

First Principles Study of Structural, Electronic and Mechanical Properties of $LiBeF_3$ under Pressure Effect

Doi: https://doi.org/10.3126/ajos.v5i1.81830

Kshitiz Kshetri[1*], Uchit Chaudhary[2], Ependra Tamang[3],
Basanta Raj Dangal[4], Abhinash Acharya[5], Kumar KC[6],
and Bhairab Sundar Singh Thakuri[7]
[1,2,3,6,7]Central Department of Physics, Tribhuvan University
[3]Faculty, Department of Science, Sukuna Multiple Campus,
[4]Patan Multiple Campus, Tribhuvan University
[5]Clarkson University
[*]Email: kkshetri16@gmail.com

Abstract

The structural, electronic and elastic properties of $LiBeF_3$ under high pressure were investigated using the density functional theory. The optimized lattice constant and the bulk modulus of elasticity at 0 GPa were obtained as 3.500 Å and 104.79 GPa, respectively, which are in good agreement with the previously available results. To study the effect of pressure, variable-cell relaxation (vc-relax) calculations were performed at different pressures ranging from 0 to 50 GPa. The mechanical properties of $LiBeF_3$ reveal that it is mechanically stable at the chosen pressures of 0, 10, 20, 30, 40 and 50 GPa. The Pugh's ratio and Poisson's ratio for $LiBeF_3$ were consistent throughout the increase in pressure, suggesting the brittle nature and dominance of ionic bonding in $LiBeF_3$. The electronic band gap of $LiBeF_3$ at 0 GPa was found to be 7.46 eV with indirect nature. On further increasing the pressure, the band gap of the $LiBeF_3$ crystal increased while maintaining its indirect nature. The Young's modulus, shear modulus and anisotropy factor of $LiBeF_3$ were also investigated and presented in this paper.

Keywords: anisotropic, non-magnetic, optoelectronics, perovskites, ultra-wide bandgap

Introduction

Perovskites are a category of materials having unique properties and their crystal structure are characterized by a chemical formula ABX_3 where A and B are cations with A larger compared to B while X represents anions (Varma, 2018).

Structurally, a perovskite is in three dimensions where B cation is surrounded by octahedron atoms and A cation is in the center of the eight octahedra cuboctahedral gap as shown in the figure 1.

Figure 1

Perovskite crystal structure

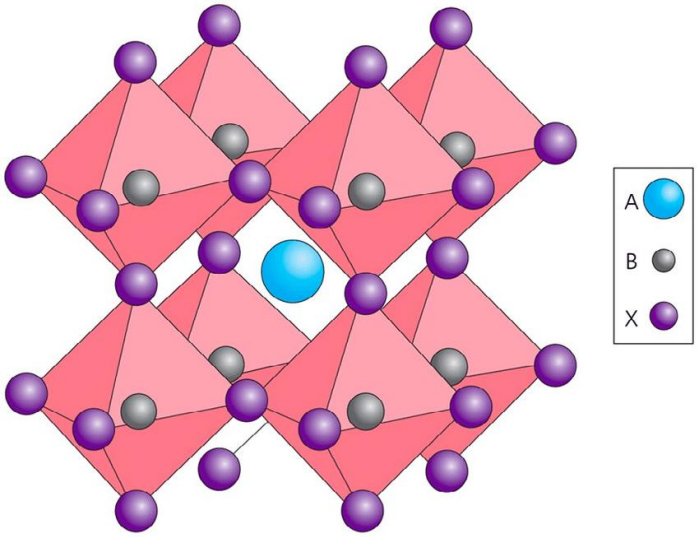

The perovskite structure is characterized by its unique arrangement of ions and its cubic symmetry, which has inspired the synthesis and study of a wide range of synthetic perovskite materials with diverse compositions and properties. Perovskite materials have several applications such as random-access memories, solar cells, sensors, supercapacitors and light emitting diodes (Kim et al., 2019; Jena, et al., 2019; Bui & Shin, 2023; Kumar et al., 2022; Fakharuddin et al., 2022). Perovskites seem to have been used extensively in technological applications these days but extensive research on perovskites and its probable applications began when Miyasaka et al. (2009;

as cited in Kojima et al., 2009) studied photovoltaic function of the organic-inorganic lead halide perovskite compounds $CH_3NH_3PbBr_3$ and $CH_3NH_3PbI_3$.

Recently, the perovskites with crystal formula ABF_3 (where A is an alkali metal and B a divalent transition metal) have been studied in considerable detail and can be used as a good base for determining further suitable half metallic complex perovskites. Complex alkali metal fluorides have received considerable attention from scientists because of their technical appeal for extended applications in organofluorochemical chemistry as fluorinating agent and as catalyst in various reactions. Fluoride-type perovskites have great potential applications such as photoluminescence, high-temperature superconductivity, colossal magneto-resistivity (CMR) (Chenine et al., 2018).

The unique properties of fluoro perovskites seems to make them useful for application in the medical field during radiation therapy and imaging plates for x-rays and gamma rays (Babu et al., 2020). Similarly, they seem to have great potential to be used in generation of energy because of their ever-increasing power conversion efficiency (Khan et al., 2023). They are also seen as probable constituents for light absorber in less toxic and high-performance perovskite solar cells and promoting cycling stability and rate capability in lithium ion batteries (Pak et al., 2023; Zhang et al., 2022).

$LiBeF_3$ in particular with its ultra-wide indirect band gap lying in the vacuum ultraviolet region, seems to be promising to be used in the field of optoelectronic and optics applications, and vacuum ultraviolet transparent material in the semiconductor industry (Benmhidi et al., 2017; Jin et al., 2019).

Syrotyuk and Shved (2014) used LDA and GW formalism to study the electronic band structure of $LiBeF_3$ and discovered that this compound has an indirect bandgap nature.

Benmhidi et. al. (2017) investigated the band structure of $LiBeF_3$ crystal by using density functional theory and showed that $LiBeF_3$ displays an indirect band gap of 7.83 eV at 0 GPa. They considered the exchange correlation potentials using the Perdew-Wang parameterization of the local density approximation (LDA). They concluded that $LiBeF_3$ is mechanically stable and they predicted that $LiBeF_3$ is a candidate vacuum-ultraviolet-transparent material for use in the semiconductor industry.

Jin et al. (2019) performed the first principles calculations of $LiBeF_3$ using the LDA and GGA-PBE functionals, and they found that $LiBeF_3$ has an indirect band gap nature with a band gap of 7.64 eV. They also studied the optical properties of $LiBeF_3$ and concluded that the absorption part of $LiBeF_3$ lies in the ultraviolet region and is suitable for optoelectronic and optics applications. To sum up, the structural, electronic, optical, thermodynamic and transport properties of $LiBeF_3$ at 0 GPa has been investigated to date.

However, the structural, electronic, mechanical, and optical properties of $LiBeF_3$ under higher pressure than ambient pressure have not been investigated yet. Good insights into these properties at higher pressures are required for the synthesis and practical applications of the compound. So, it is necessary to study these basic properties of $LiBeF_3$ crystals at higher pressure. In this research, the Projector Augmented Wave (PAW) (Blöchl, 1994) based on density functional theory (DFT) (Hohenberg & Kohn, 1964; Kohn & Sham, 1965) was used to investigate the structural, electronic and elastic properties of $LiBeF_3$ at pressures ranging from 0 to 50 GPa. The modulation of pressure on different properties of the $LiBeF_3$ presented in this paper would serve as a theoretical framework for the synthesis and application of $LiBeF_3$ in the near future.

Methods and Materials

The structural, electronic and mechanical properties of a $LiBeF_3$ unit cell were investigated based on the first principles technique. The calculations are performed

using density functional theory and the projector augmented wave (PAW) technique using the Perdew–Burke–Ernzerhof (PBE) (Perdew et al., 1996; Perdew et al., 1997) exchange–correlation functional. Quantum Espresso (QE) (Giannozzi et al., 2009; Giannozzi et al., 2017) code was used to perform the DFT calculations. The Brillouin zone was sampled through a Monkhorst-Pack (Monkhorst & Pack, 1976), 8x8x8 k-point mesh, and the cut-off energy was set to 100 Rydbergs. An extension to the quantum ESPRESSO, thermo_pw (Corso, 2014) was implemented for the approximation of elastic properties. All the properties of $LiBeF_3$ discussed in this paper were estimated for a unit cell of $LiBeF_3$ under the external isotropic pressure of 10, 20, 30, 40 and 50 GPa, including the ambient pressure of 0 GPa.

Result and Discussion

Structural and Elastic properties

Figure 2

Unit cell of $LiBeF_3$

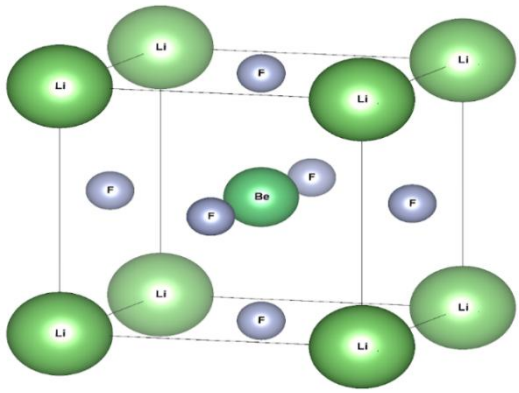

$LiBeF_3$ consists of a cubic unit cell lying in the Pm-3m space group. The unit cell of $LiBeF_3$ is represented in figure 2. The Li atom is positioned at (0.0, 0.0, 0.0); similarly, the Be atom is situated at (0.5, 0.5, 0.5) and the F atoms are located at (0.0, 0.5, 0.5), (0.5, 0.0, 0.5), and (0.5, 0.5, 0.0), respectively. The unit cell of $LiBeF_3$ was optimized using the PBE functional and it was found that the energy of its nonmagnetic state was lower

than the ferromagnetic state. Thus, it was assured that $LiBeF_3$ exists in a non-magnetic state, which was already proven by the previously available literature as well. Taking it into account, the further calculations in this research paper of $LiBeF_3$ is performed for the non-magnetic state.

The optimized lattice parameter of $LiBeF_3$ at 0 GPa and 0 K was found to be 3.500 Å. However, the lattice parameter of cubic $LiBeF_3$ decreased to 3.405, 3.336, 3.280, 3.235 and 3.194 Å on applying the pressure of 10, 20, 30, 40 and 50 GPa, respectively.

The formation and cohesive energy were calculated to check the chemical stability of the compound at 0 GPa. The formation and cohesive energy of $LiBeF_3$ can be expressed (Ray et al., 2024) as,

$$E_{for} = E_{LiBeF_3}^{total} - (E_{Li}^{bulk} + E_{Be}^{bulk} + 3E_F^{bulk}) \quad (1)$$

$$E_{coh} = E_{LiBeF_3}^{total} - (E_{Li}^{iso} + E_{Be}^{iso} + 3E_F^{iso}) \quad (2)$$

E_{for} and E_{coh} stand for the formation energy and cohesive energy of $LiBeF_3$, while E^{bulk} and E^{iso} are respectively total energy per atom in bulk and single isolated form of Li, Be and F. The formation energy and cohesive energy were observed to be -4.10 eV and -4.87 eV respectively. The negative formation energy and the negative cohesive energy point towards the energetic stability of the compound and it can be concluded that the compound can be extracted chemically in typical conditions.

Further, to assure mechanical stability, the elastic constants of the material should satisfy Born criteria (Born & Huang, 1954). For a cubic system, three independent elastic constants (C_{11}, C_{12}, and C_{44}) should satisfy the three conditions initially proposed by Born in 1954: $C_{11} - C_{12} > 0$; $C_{11} + 2C_{12} > 0$; $C_{44} > 0$.

The calculated elastic constants at various pressures are presented in Tables 1 and 2 and it is clear that these parameters satisfy the criteria for mechanical stability of $LiBeF_3$ at all the considered pressures. The independent elastic constants C_{11} and C_{33} suggest the response of the solid to uniaxial strain and the elastic constant C_{44} describes the resistance

towards shape deformation. The higher C_{11} and C_{12} in comparison to C_{44} indicate the lesser resistance of $LiBeF_3$ towards the shear deformation as compared to a uniaxial deformation.

The elastic constants can also be applied to determine various other elastic properties of materials. Bulk modulus, Shear modulus, Young's modulus and Poisson's ratio can be estimated using Voigt, Reuss and Hill estimations (Voigt, 1966; Hill, 1952; Reuss, 1929). In the cubic systems, the Voigt and Reuss bulk modulus of elasticity are equal (deWit, 2008), and it can be expressed as,

$$B = \frac{1}{3}(C_{11} + 2C_{12}) \quad (3)$$

The Voigt shear modulus (G_V) and Reuss shear modulus of elasticity (G_R) in terms of elastic constants C_{11}, C_{12} and C_{44} are:

$$G_{\square} = \frac{1}{5}(C_{11} - C_{12} + 3C_{44}) \quad (4)$$

$$G_{\square} = \frac{5C_{44}\,(C_{11} - C_{12})}{4C_{44} + 3\,(C_{11} - C_{12})} \quad (5)$$

The actual modulus of elasticity is approximated as the arithmetic mean of these values by Hill as

$$G = \frac{1}{2}(G_V + G_R) \quad (6)$$

And the Young's modulus of elasticity (E) and Poisson's ratio (ν) are estimated using the Bulk modulus of elasticity and Shear modulus of elasticity,

$$E = \frac{9BG}{(3B + G)} \quad (7)$$

$$\nu = \frac{(3B - 2G)}{2(3B + G)} \quad (8)$$

Table 1

Obtained Value of a_0, C_{11}, C_{12}, C_{44}, B_0, E, G, E_{for}, E_{coh} at 0 GPa and 0 K

a_0 (Å)	C_{11} (GPa)	C_{12} (GPa)	C_{44} (GPa)	B_0 (GPa)	E (GPa)	G (GPa)	E_{for} (eV)	E_{coh} (eV)
3.500	136.53	88.92	81.03	104.79	128.36	49.72	- 4.10	- 4.87
3.424[a]				117.88[a]	154.34[a]	60.21[a]		
3.466[b]				111.64[b]		61.40[b]		
3.515[b]				119.05[b]		56.29[b]		
3.482[c]								

[a] Theoretical (Benmhidi et al., 2017), [b] Theoretical (Jin et al., 2019), [c] Theoretical (Flocken et al., 1985)

The lattice constant, elastic constants, bulk modulus, Young's modulus, shear modulus, cohesive energy and formation energy of $LiBeF_3$ at ambient pressure 0 GPa and temperature 0 K along with the previously available data

Table 2

The lattice constant, elastic constants, bulk modulus, Young's modulus and shear modulus of $LiBeF_3$ at various pressures

Pressure (GPa)	a_0 (Å)	C_{11} (GPa)	C_{12} (GPa)	C_{44} (GPa)	B (GPa)	E (GPa)	G (GPa)
0	3.500	136.53	88.92	81.03	104.79	128.36	49.72
10	3.405	136.64	88.98	81.06	104.86	128.45	49.76
20	3.336	137.38	89.34	81.23	105.36	129.02	49.97

30	3.280	138.81	90.01	81.55	106.27	130.15	50.40
40	3.234	140.47	90.80	81.96	107.35	131.43	50.89
50	3.194	142.25	91.65	82.34	108.52	132.80	51.41

The Pugh ratio (G/B) is crucial in extracting information regarding the brittleness of a material (Pugh, 1954). The critical value is 0.57 for Pugh's ratio. It is observed that materials having Pugh's ratio greater than 0.57 exhibit a ductile nature and a brittle nature for Pugh's ratio lower than 0.57. In the case of $LiBeF_3$, Pugh's ratio was found to be 0.47 at 0 GPa, and on increasing the pressure, significant changes in the ratio were not observed. Thus, it can be supposed that $LiBeF_3$ is brittle in nature for all the considered pressure ranges.

Similar to Pugh's ratio, Poisson's ratio can be used to estimate the nature of bonding in the compound. For a poisson's ratio less than 0.25, the compound is said to have covalent bonding, and the compound is considered to possess ionic bonding for the value of a Poisson's ratio greater than 0.25. Like the Pugh's ratio, the Poisson's ratio of $LiBeF_3$ was too found to be constant throughout the increasing pressure and it was recorded to be 0.29 for all the pressure ranges. Since the obtained values are greater than the critical Poisson's ratio, it can be said that $LiBeF_3$ is dominated by ionic bonding.

There is a parameter called elastic anisotropy that explains whether the elastic properties of material vary with direction. It may affect various physical properties of materials. The anisotropy factor proposed by Zener (Zener, 1948), depending on elastic constants C_{11}, C_{12} and C_{44} is given by,

$$A = \frac{2C_{44}}{C_{11}-C_{12}} \qquad (9)$$

The value of the anisotropy factor should be 1 for a perfect isotropic material, while any value different than 1 represents anisotropy in the material. The anisotropy

factor for $LiBeF_3$ is presented in table 2. The anisotropy factor was obtained to be 3.40 for 0 GPa and it gradually decreased till it reached 3.25 for 50 GPa but its value was nowhere near 1. So, it can be easily inferred that $LiBeF_3$ is anisotropic, and its physical properties vary with direction.

Table 3

The Pugh' ratio, Poisson's ratio and anisotropy factors of $LiBeF_3$ at different pressures

Pressure (GPa)	n	ν	A
0	0.47	0.29	3.40
10	0.47	0.29	3.40
20	0.47	0.29	3.38
30	0.47	0.29	3.34
40	0.47	0.29	3.30
50	0.47	0.29	3.25

Electronic Properties

Figure 3

Band structures of $LiBeF_3$ at pressures ranging from 0 to 50 GPa

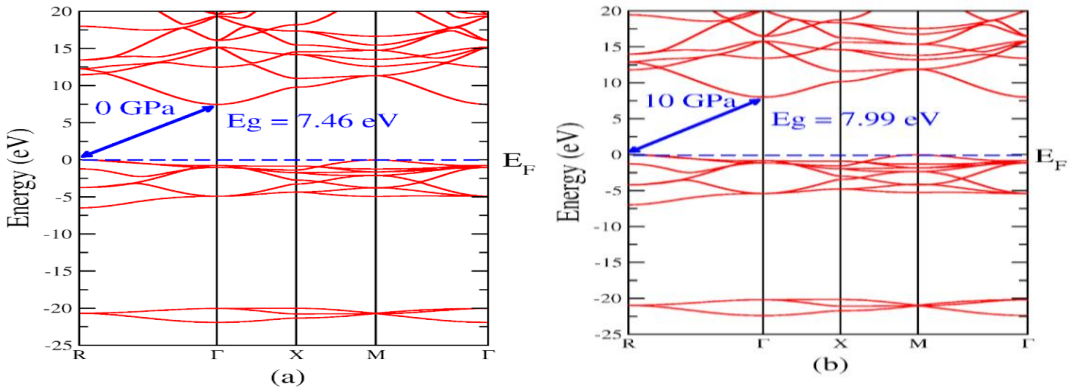

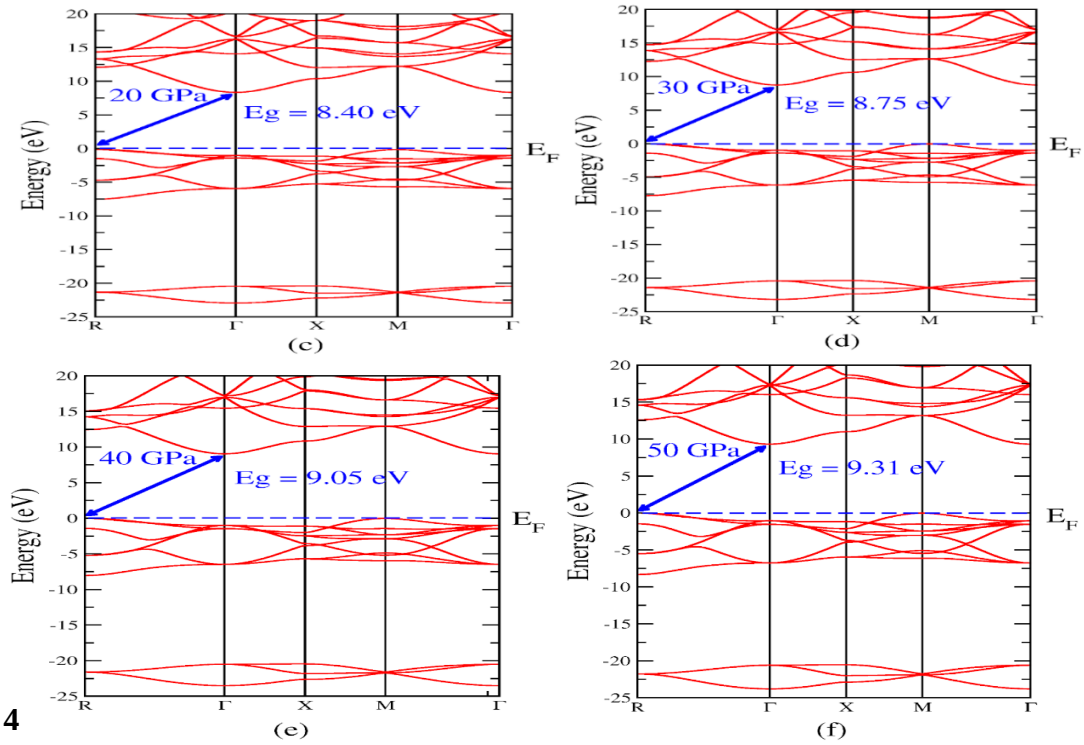

Table 4

Band gaps of $LiBeF_3$ at pressure range of 0 to 50 GPa

Pressure (GPa)	Band Gap (eV)
0	7.46, 7.83[a], 7.26[b], 7.27[b], 7.64[b], 8.52[c], 7.73[d],
10	7.99
20	8.40
30	8.75
40	9.05
50	9.31

[a] Theoretical (Benmhidi et al., 2017), [b] Theoretical (Jin et al., 2019)

[c] Theoretical (Syrotyuk & Shved, 2014), [d] Theoretical (Nishimatsu et al., 2002)

To determine the electronic properties and study its composition, the band structure calculations of $LiBeF_3$ at different pressures are performed and plotted in figure 3. The dotted line at the energy level of 0 eV represents the fermi level and conduction and valence bands lie on either side of the fermi level, with the valence band below the fermi level and the conduction band present above the fermi level. From band structure observation, it can be seen that the valence band maximum of $LiBeF_3$ lies at the symmetry point R while the conduction band minimum lies at the point Γ thus indicating towards the indirect band gap. The band gap of $LiBeF_3$ at 0 GPa was found to be 7.46 eV which is in excellent agreement with the previously available results. With such a large value of band gap, $LiBeF_3$ can be referred to as an insulating material. On increasing the pressure from 0 to 50 GPa, the band gap of $LiBeF_3$ further increases gradually. However, it is found that $LiBeF_3$ maintains its indirect band gap nature throughout the increment of pressure. On increasing the pressure, the lattice constant decreases and the electron transition integral rises. As a result, the energy band gap of $LiBeF_3$ increases on changing the pressure positively. Different values of band gaps obtained at various pressures are presented in Table 4.

For deeper insights into the band structure of $LiBeF_3$, the density of states of $LiBeF_3$ indicating the contribution from individual atoms was calculated for different pressures, which are presented in figure 4. In 0 GPa pressure, as shown in figure 4 (a), the bottom of the valence band ranging from -21.91 to -20.00 eV is mainly derived from the F-2s and Be-2p states with minor contributions from the Li-2p and Be-2s states. A hybridization is observed between these states. In the second region, ranging from -6.46 to 0 eV, a significant contribution appears to be from the F-2p state, with smaller contributions from the Li-2p, Be-2s and Be-2p states. Hybridization is observed in this region as well.

Similarly, the third region existing between 7.51 eV and 16.66 eV above the fermi level is mainly composed of 2s and 2p states of Li and Be with main contributions from

Li-2p. At the end, in the fourth region lying at 16.66 eV and beyond, a sharp peak is observed by the main contribution from the 2p state of Be and a small contribution from the 2s state of Be. Minute contributions from the 2p state of Li and 2p state of F are also observed in this region. It can be seen that the Li-2p state gradually shifts away from the fermi level on increasing the pressure. As a result, the band gap increases.

Figure 4

Density of states of $LiBeF_3$ at pressures ranging from 0 to 50 GPa

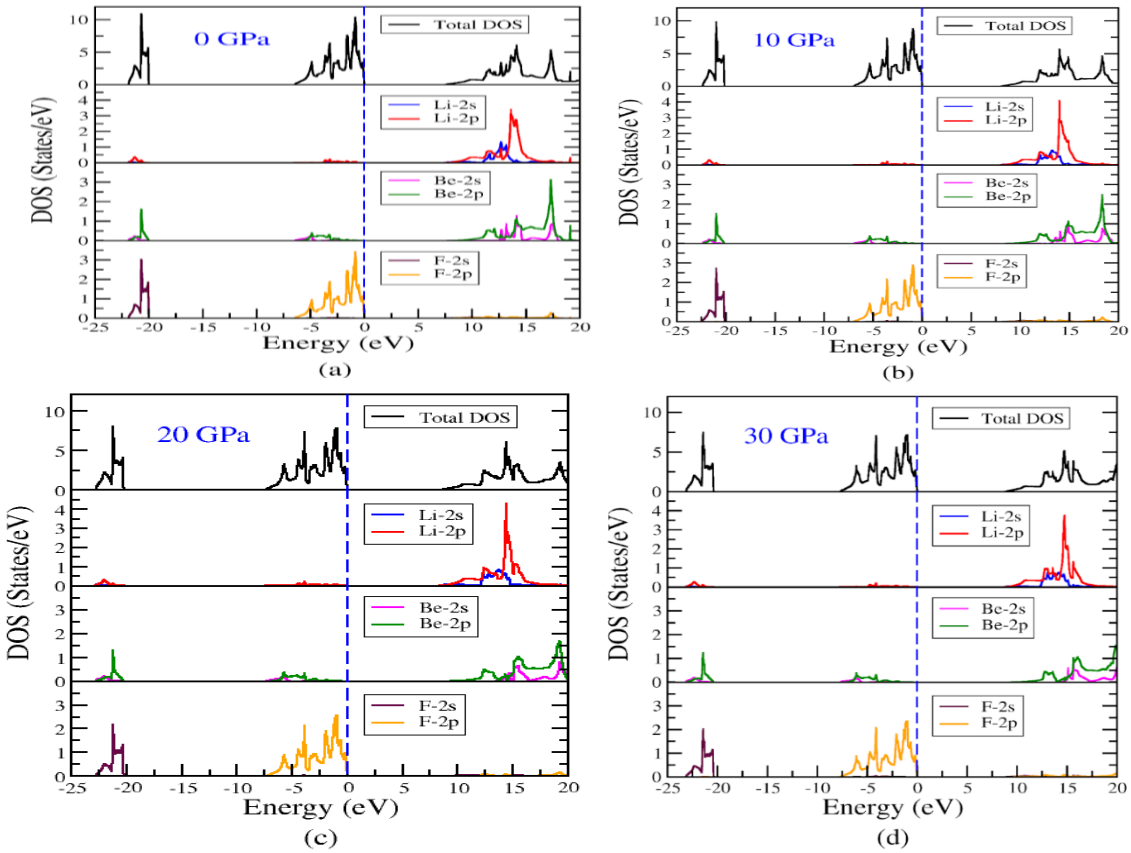

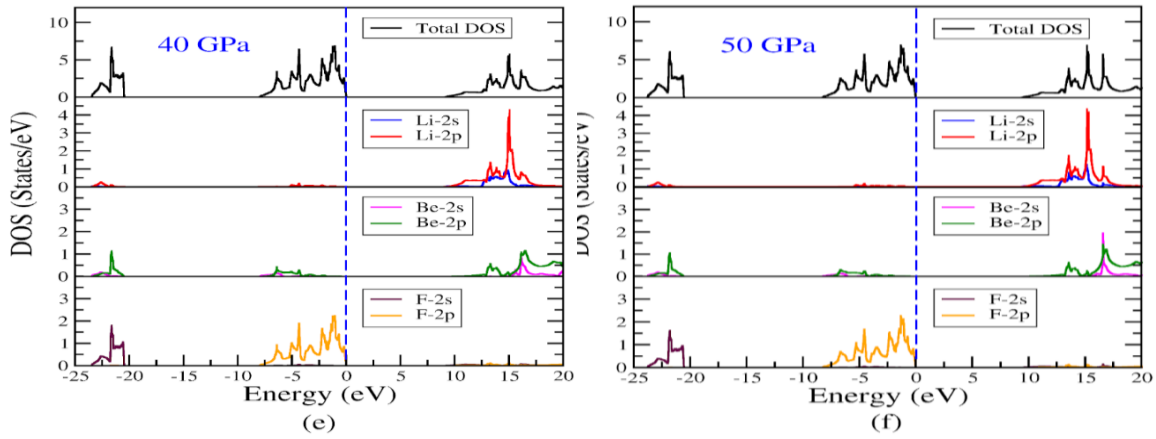

Conclusion

The structural, mechanical and electronic properties of $LiBeF_3$ were investigated at various pressures using the PAW-PBE method under the framework of density functional theory. The calculated structural parameters, moduli of elasticity and band gap at 0 GPa are consistent with the previously available results. However, the obtained values at higher pressures could not be compared due to the lack of data. From the calculation of structural properties, it was observed that the lattice parameter of $LiBeF_3$ decreases with increasing the pressure and the analysis of mechanical properties reveals that $LiBeF_3$ is mechanically stable at the pressure range from 0 to 50 GPa. The electronic property of $LiBeF_3$ points out that the band gap of $LiBeF_3$ at ambient 0 GPa pressure is 7.46 eV and on further increasing the pressure, the band gap of $LiBeF_3$ increases and becomes 9.31 eV at 50 GPa. Thus, the band gap of $LiBeF_3$ lies in the ultraviolet region and $LiBeF_3$ can be used in optoelectronics and it can also be considered as a promising candidate for vacuum-ultraviolet-transparent lens material in optical lithography. In this research, Pugh's ratio and Poisson's ratio were also determined. Through the analysis of Pugh's ratio, it was revealed that the $LiBeF_3$ crystal is brittle in nature and it does not lose the

brittleness on increasing pressure. Similarly, through the Poisson's ratio, it can be seen that the bonding $LiBeF_3$ is ionic predominantly.

Furthermore, the observed pressure-induced widening of the band gap in $LiBeF_3$ contributes valuable insights to the design and development of ultra-wide bandgap (UWBG) materials. Such materials are highly relevant in extreme-environment optoelectronics, ultraviolet photodetectors, and radiation-hardened devices. The increasing band gap under compression suggests potential applications in UV-transparent optical components, including high-pressure windows and lenses for deep-ultraviolet (DUV) lithography.

References

Babu, K. E., Neeraja, K., Deenabandhu, D., Ratna, A. M. V., Kumar, V. V., Kumari, K. B., Taddesse, P., Aregai, G. T., Mehar, M.V.K, Babu, B. V., Samatha, K. & Veeraiah, V. (2020). First-principles study of structural, elastic, electronic and optical properties of cubic perovskite LiMgF3 for novel applications. *Journal of Physics: Conference Series, 1495*(1), 012010. https://doi.org/10.1088/1742-6596/1495/1/012010

Benmhidi, H., Rached, H., Rached, D., & Benkabou, M. (2017). Ab initio study of electronic structure, elastic and transport properties of fluoroperovskite LiBeF3. *Journal of Electronic Materials, 46*(4), 2205–2210. https://doi.org/10.1007/s11664-016-5159-0

Blöchl, P. E. (1994). Projector augmented-wave method. *Physical Review B, 50*(24), 17953–17979. https://api.semanticscholar.org/Corpus ID:43534257

Born, M., & Huang, K. (1954). *Dynamical theory of crystal lattices*. Oxford University Press. https://api.semanticscholar.org/CorpusID:59567814

Bui, T. H., & Shin, J. H. (2023). Perovskite materials for sensing applications: Recent advances and challenges. *Microchemical Journal, 191*, 108924. https://doi.org/10.1016/j.microc.2023.108924

Chenine, D., Aziz, Z., Benstaali, W., Bouadjemi, B., Youb, O., Lantri, T., Abbar, B. & Bentata, S. (2018). Theoretical investigation of half-metallic ferromagnetism in sodium-based fluoro-perovskite NaXF3 (X = V, Co). *Journal of Superconductivity and Novel Magnetism, 31*, 1927–1934. https://doi.org/10.1007/s10948-017-4204-4

Corso, A. D. (2014). *thermo_pw* [Computer software]. Thermo_pw user's guide (v.1.6.1).

deWit, R. (2008). Elastic constants and thermal expansion averages of a nontextured polycrystal. *Journal of Mechanics of Materials and Structures, 3*(1), 195–212. https://doi.org/10.2140/jomms.2008.3.195

Fakharuddin, A., Gangishetty, M. K., Abdi-Jalebi, M., Chin, S. H., Bin Mohd Yusoff, A. R., Congreve, D. N., Tress, W., Deschler, F., Vasilopoulou, M. & Bolink, H. J. (2022). Perovskite light-emitting diodes. *Nature Electronics, 5*(4), 203–216. https://doi.org/10.1038/s41928-022-00745-7

Flocken, J. W., Guenther, R. A., Hardy, J. R., & Boyer, L. L. (1985). First-principles study of structural instabilities in halide-based perovskites: Competition between ferroelectricity and ferroelasticity. *Physical Review B, 31*(12), 7252–7260. https://digitalcommons.unl.edu/physicshardy/37

Giannozzi, P., Andreussi, O., Brumme, T., Bunau, O., Nardelli, M. B., Calandra, M., Car, R., Cavazzoni, C., Ceresoli, D., Cococcioni, M, Colonna, N., Carnimeo, I., Corso, A. D., Gironcoli, S., Delugas, P., DiStasio, R. A., Ferretti, A., Floris, A., Fratesi, G., . Baroni, S. (2017). Advanced capabilities for materials modelling with Quantum ESPRESSO. *Journal of Physics: Condensed Matter, 29*(46), 465901. https://doi.org/10.1088/1361-648X/aa8f79

Giannozzi, P., Baroni, S., Bonini, N., Calandra, M., Car, R., Cavazzoni, C., Ceresoli, D., Chiarotti, G. L., Cococcioni, M., Dabo, I., Corso, A. D., Gironcoli, S., Fabris, S., Fratesi, G., Gebauer, R., Gerstmann, U., Gougoussis, C., Kokalj, A., Lazzeri, M., . . . Wentzcovitch, R. M. (2009). QUANTUM ESPRESSO: A modular and

open-source software project for quantum simulations of materials. *Journal of Physics: Condensed Matter, 21*(39), 395502. https://doi.org/10.1088/0953-8984/21/39/395502

Hill, R. (1952). The elastic behaviour of a crystalline aggregate. *Proceedings of the Physical Society. Section A, 65*, 349–354. https://doi.org/10.1088/0370-1298/65/5/307

Hohenberg, P., & Kohn, W. (1964). Inhomogeneous electron gas. *Physical Review, 136*(3B), B864–B871. https://doi.org/10.1103/PhysRev.136.B864

https://people.sissa.it/~dalcorso/thermo_pw/ug.1.6.1.pdf

Jena, A. K., Kulkarni, A., & Miyasaka, T. (2019). Halide perovskite photovoltaics: Background, status, and future prospects. *Chemical Reviews, 119*(5), 3036–3103. https://doi.org/10.1021/acs.chemrev.8b00539

Jin, Z., Wu, Y., Li, S., Chen, S., Zhang, W., Wu, Q., & Zhang, C. (2019). First-principles calculation of the electronic structure, optical, elastic and thermodynamic properties of cubic perovskite LiBeF3. *Materials Research Express, 6*(12), 126309. https://doi.org/10.1088/2053-1591/ab5edc

Khan, H., Sohail, M., Arif, M. S., & Abodayeh, K. (2023). Insight into the physical properties of fluoro-perovskites compounds of Tl-based TlMF3 (M = Au, Ga) compounds studied for energy generation utilizing the TB-MBJ potential approximation approach. *Materials, 16*(2), 686. https://doi.org/10.3390/ma16020686

Kim, H., Han, J. S., Kim, S. G., Kim, S. Y., & Jang, H. W. (2019). Halide perovskites for resistive random-access memories. *Journal of Materials Chemistry C, 7*(18), 5226–5234. https://doi.org/10.1039/C8TC06031B

Kohn, W., & Sham, L. J. (1965). Self-consistent equations including exchange and correlation effects. *Physical Review, 140*(4A), A1133–A1138. https://doi.org/10.1103/PhysRev.140.A1133

Kojima, A., Teshima, K., Shirai, Y., & Miyasaka, T. (2009). Organometal halide perovskites as visible-light sensitizers for photovoltaic cells. *Journal of the American Chemical Society, 131*(17), 6050–6051. https://doi.org/10.1021/ja809598r

Kumar, R., Kumar, A., Shukla, P. S., Varma, G. D., Venkataraman, D., & Bag, M. (2022). Photorechargeable hybrid halide perovskite supercapacitors. *ACS Applied Materials & Interfaces, 14*(31), 35592–35599. https://doi.org/10.1021/acsami.2c07440

Monkhorst, H. J., & Pack, J. D. (1976). Special points for Brillouin-zone integrations. *Physical Review B, 13*(12), 5188–5192. https://doi.org/10.1103/PhysRevB.13.5188

Nishimatsu, T., Terakubo, N., Mizuseki, H., Kawazoe, Y., Pawlak, D. A., Shimamura, K., & Fukuda, T. (2002). Band structures of perovskite-like fluorides for vacuum-ultraviolet-transparent lens materials. *Japanese Journal of Applied Physics, 41*(Part 2, No. 4A), L365–L367. https://doi.org/10.1143/jjap.41.l365

Pak, C. J., Jong, U. G., Kang, C. J., Kim, Y. S., Kye, Y. H., & Yu, C. J. (2023). First-principles study on the optoelectronic and mechanical properties of all-inorganic lead-free fluoride perovskites ABF3 (A = Na, K and B = Si, Ge). *Materials Advances, 4*, 4528–4536. https://doi.org/10.1039/d3ma00457k

Perdew, J. P., Burke, K., & Ernzerhof, M. (1996). Generalized gradient approximation made simple. *Physical Review Letters, 77*(18), 3865–3868. https://doi.org/10.1103/PhysRevLett.77.3865

Perdew, J. P., Burke, K., & Ernzerhof, M. (1997). Generalized gradient approximation made simple (Erratum). *Physical Review Letters, 78*(7), 1396. https://doi.org/10.1103/PhysRevLett.78.1396

Pugh, S. F. (1954). XCII. Relations between the elastic moduli and the plastic properties of polycrystalline pure metals. *The London, Edinburgh, and Dublin Philosophical*

Magazine and Journal of Science, 45(367), 823–843. https://doi.org/10.1080/14786440808520496

Ray, R. B., Rai, R. K., Yadav, D. K., & Kaphle, G. C. (2024). Exploring FeMnVAl Heusler alloy: Physical, mechanical, and magnetic properties. *Journal of Lumbini Engineering College, 6*(1), 93–104. https://doi.org/10.3126/lecj.v6i1.66288

Reuss, A. (1929). Calculation of the flow limits of mixed crystals on the basis of the plasticity of monocrystals. *Zeitschrift für Angewandte Mathematik und Mechanik* [Journal of Applied Mathematics and Mechanics], *9*(1), 49–58. https://doi.org/10.1002/zamm.19290090104

Syrotyuk, S., & Shved, V. (26-30 May 2014). *Quasiparticle electronic band structure of the cubic LiBeF3 crystal* [Conference Paper]. IEEE International Conference on Oxide Materials for Electronic Engineering (OMEE). Doi**:** 10.1109/OMEE.2014.6912336

Varma, P. C. R. (2018). Low-dimensional perovskites. In S. Thomas & A. Thankappan (Eds.), *Perovskite photovoltaics* (pp. 197–229). Elsevier. https://doi.org/10.1016/B978-0-12-812915-9.00007-1

Voigt, W. (1966). *Lehrbuch der Kristallphysik [*Textbook of crystal physics (excluding crystal optics)]. Springer Nature Link. https://doi.org/10.1007/978-3-663-15884-4

Zener, C. (1948). *Elasticity and anelasticity of metals*. University of Chicago Press.

Zhang, Y., Liu, Y., Zhou, J., Wang, D., Tan, L., & Yi, C. (2022). 3D cubic framework of fluoride perovskite SEI inducing uniform lithium deposition for air-stable and dendrite-free lithium metal anodes. *Chemical Engineering Journal, 431*, 134266. https://doi.org/10.1016/j.cej.2021.134266